

**Signal Transduction:**

**A conserved phenylalanine as relay  
between the  $\alpha 5$  helix and the GDP binding  
region of heterotrimeric Gi protein  $\alpha$   
subunit**



Ali I. Kaya, Alyssa D. Lokits, James A.  
Gilbert, Tina M. Iverson, Jens Meiler and  
Hamm E. Hamm  
*J. Biol. Chem.* published online July 18, 2014

Access the most updated version of this article at doi: [10.1074/jbc.M114.572875](https://doi.org/10.1074/jbc.M114.572875)

Find articles, minireviews, Reflections and Classics on similar topics on the [JBC Affinity Sites](#).

Alerts:

- [When this article is cited](#)
- [When a correction for this article is posted](#)

[Click here](#) to choose from all of JBC's e-mail alerts

This article cites 0 references, 0 of which can be accessed free at  
<http://www.jbc.org/content/early/2014/07/18/jbc.M114.572875.full.html#ref-list-1>

A conserved phenylalanine as a relay between the  $\alpha 5$  helix and the GDP binding region of heterotrimeric G $\alpha$  protein  $\alpha$  subunit\*

Ali I. Kaya<sup>1</sup>, Alyssa D. Lokits<sup>2</sup>, James A. Gilbert<sup>1</sup>, Tina M. Iverson<sup>1,3</sup>, Jens Meiler<sup>1,4</sup> and Heidi E. Hamm<sup>1</sup>

From the <sup>1</sup>Department of Pharmacology, the <sup>2</sup>Department of Neuroscience, the <sup>3</sup>Department of Biochemistry and the <sup>4</sup>Department of Chemistry, Vanderbilt University Medical Center, Nashville, Tennessee 37232

\*Running title: G protein  $\alpha 5$  helix relays stability to GDP binding region

To whom correspondence should be addressed: Department of Pharmacology; 442 Robinson Research Building; Vanderbilt University Medical Center, Nashville, TN 37232-6600. Tel: 615-343-3533; Fax: 615-343-1084; Email: Heidi.hamm@vanderbilt.edu

**Keywords:** Heterotrimeric G protein; G protein Coupled Receptors (GPCR); Computer modeling; Rhodopsin; Protein conformation; Signal transduction; GDP release

**Background:** GPCRs regulate heterotrimeric G protein activation, however the intermediate steps regulating GDP release are still unknown.

**Results:** Energy analysis pinpoints information flow through G $\alpha$ -receptor interaction and GDP release.

**Conclusion:** Hydrophobic interactions around  $\alpha 5$  helix,  $\beta 2$ - $\beta 3$  strands and  $\alpha 1$  helix are key for GDP stability.

**Significance:** G protein activation defines regulation of high affinity receptor interactions and plays a role defining different cellular responses.

## ABSTRACT

G protein activation by G protein coupled receptors (GPCRs) is one of the critical steps for many cellular signal transduction pathways. Previously, we and other groups reported that the alpha 5 ( $\alpha 5$ ) helix in the G protein alpha subunit plays a major role during this activation process. However, the precise signaling pathway between the  $\alpha 5$  helix and the GDP binding pocket remains elusive. Here, using structural, biochemical and computational techniques, we probed different residues around the  $\alpha 5$  helix for their role in signaling. Our data showed that perturbing the F336 ( $\alpha 5$ ) residue disturbs hydrophobic interactions with the  $\beta 2$ - $\beta 3$  strands and  $\alpha 1$  helix,

leading to high basal nucleotide exchange. However, mutations in  $\beta$  strands  $\beta 5$  and  $\beta 6$  do not perturb G protein activation. We have highlighted critical residues that leverage F336 as a relay. Conformational changes are transmitted starting from F336 via  $\beta 2$ - $\beta 3/\alpha 1$  to Switch I and the P-loop, decreasing the stability of the GDP binding pocket and triggering nucleotide release. When the  $\alpha 1$  and  $\alpha 5$  helices were cross-linked, inhibiting the receptor-mediated displacement of the C-terminal  $\alpha 5$  helix, mutation of F336 still leads to high basal exchange rates. This suggests that unlike receptor mediated activation, helix 5 rotation and translocation is not necessary for GDP release from the  $\alpha$  subunit. Rather, destabilization of the backdoor region of the G $\alpha$  subunit is sufficient for triggering the activation process.

Heterotrimeric G proteins play a critical role as molecular switch proteins that couple the activation of cell surface receptors, G protein coupled receptors (GPCRs), to different intracellular effector proteins mediating intracellular responses. Therefore, G proteins have a crucial role in defining the specificity and temporal characteristics of many different cellular responses (1-5).

Several structural and biophysical studies have proposed the conformation of the receptor in its

active state and have identified potential receptor mediated mechanisms for G protein activation and GDP release (6-16). Two well-studied receptor mediated G protein activation routes have been hypothesized. In the first, the binding of the GPCR to the C-terminus (CT) of  $G\alpha$  is thought to trigger conformational changes that can be transmitted via rotation of the  $\alpha 5$  helix of  $G\alpha$  to the  $\beta 6$ - $\alpha 5$  turn on the purine ring of the GDP (**Fig. 1**) (3,9,17-19). In the second proposed mechanism, the GPCR is thought to take advantage of  $G\beta\gamma$  as a nucleotide exchange factor in order to disrupt the phosphate interactions of the nucleotide binding pocket via destabilization of switch (SW) I-II regions through perturbing  $\alpha 5$  interaction with the  $\beta 2$ - $\beta 3$  strands (**Fig. 1**) (20-25).

In 2011, Kobilka and colleagues provided an important missing piece of the puzzle in the receptor mediated G protein activation cycle by determining the structure of the  $\beta 2$ -adrenergic receptor -  $G_s$  heterotrimer complex ( $\beta 2$ AR- $G_s$ ) structure (18). This ground-breaking study detailed the receptor - G protein (R-G) interaction and G protein activation. This structure represents the end point in the signal transduction step. The signaling route by which an active receptor interacts with an inactive G protein and causes conformational changes that lead to the final high-affinity complex of a receptor with its cognate G protein and GDP release is still unknown.

To address the conformational dynamics underlying nucleotide release from the  $G\alpha$  subunit, we recently generated a predictive computational model of the energy of receptor activation with the goal of understanding conformational changes and connections between potential key residues during G protein activation (26). In this model of the rhodopsin -  $G\alpha\beta\gamma$  complex, it was suggested that the  $\alpha 5$  helix is the most critical region for G protein stability and activation, and is consistent with previous studies (9,12,14,15,27). The  $\alpha 5$  helix is protected and surrounded with primarily hydrophobic interactions within six beta strands ( $\beta 1$ - $\beta 6$ ) and one alpha helix ( $\alpha 1$ ) (**Fig. 1C & D**). Energetic analysis predicted that residues F191, F196 in  $\beta 2$ - $\beta 3$ ; I265, F267 in  $\beta 5$ ; Y320, H322 in  $\beta 6$  strands; Q52 and M53 in the  $\alpha 1$  helix are making critical interaction with the  $\alpha 5$  helix in both basal and receptor mediated G protein activation (26). These key residues might either be important for the overall structural integrity of the

GTPase domain during the activation process, or they may be directly involved in activation.

In order to identify the residue-residue interactions that are critical for activation as a part of the signaling pathway, we systematically tested the effects of these residue-residue interactions on G protein activation. Residues were examined using biochemical, computational, and structural approaches in both basal and receptor bound states. In this study, recombinant  $G\alpha i 1$  was used for all experiments instead of visual G protein, given that  $G\alpha i 1$  is a very close homolog of  $G\alpha t$  yet much more easily expressed in *E.coli*. Our data showed that single mutations in the  $\beta 5$  and  $\beta 6$  strands that face the  $\alpha 5$  helix were not able to break hydrophobic interactions and trigger GDP release from G protein in both receptor bound and unbound states. In the receptor bound state, using pairwise coupling energy analysis, we predicted that the  $\alpha 5$  rotation compensates the effect of  $\beta 5$ - $\beta 6$  mutations on protein activation.

However, the hydrophobic interactions on the opposite side of the  $\alpha 5$  helix were predicted to directly affect G protein function. Energetic analysis predicted that phenylalanine 336 (F336) is the most critical residue in the  $\alpha 5$  helix; it creates a hydrophobic hotspot of G protein activation, consistent with previous studies (14,28,29). The amplitude of this effect was correlated with decreasing hydrophobicity of the side chain. Experimentally tracing the hydrophobic interactions around the F336 residue together with computational analysis provided evidence for a dynamic interplay between F336, the  $\beta 2$  and  $\beta 3$  strands, and the  $\alpha 1$  helix on the G protein activation route.

## EXPERIMENTAL PROCEDURES

*Materials*- The TSKgel G2000SW column, GDP, and guanosine 5'-O-(3-thiotriphosphate) tetralithium salt (GTP $\gamma$ S) were purchased from Sigma. All other reagents and chemicals were of the highest available purity.

*Rosetta interface energy calculations*- Interface energies were computed following the Rosetta  $\Delta\Delta G$  protocol previously described (26). Briefly: we leveraged the previously published ensembles of ten structures of the G-protein in the basal state and receptor bound state. Residue-residue interactions across  $\alpha 1$  helix/GTPase domain interface were evaluated by measuring

energetic perturbations when computationally removing the  $\alpha 1$  helices from the models. The  $\alpha 1$  helix was defined as residues 45 to 58. For all analyses, GDP remained fixed within the nucleotide binding pocket. The  $\Delta\Delta G$  value is reported as an average over the ten structural models in Rosetta Energy Units (REU). Absolute values larger than 0.5 REU are considered to be significant. Using the standard deviation over the ten structures a Z-score was computed. The total  $\Delta\Delta G$ -value across the interface is calculated as the sum of individual residue contributions.

*Rosetta pairwise binding energy calculations*- Average energies between pairwise interacting residues were computed using Rosetta's per residue energy-breakdown protocol. The energy between all possible pairs of interacting amino acid residues within the G-protein were calculated across the previously published ensembles of ten structures (26). These energies between all residues pairs was then averaged across the ten models in both the receptor bound and basal state. Predicted energy values are reported in Rosetta Energy Units (REU) and considered significant if greater than 0.5 REU.

*Preparation of urea washed ROS membranes and G $\beta 1\gamma 1$* - Urea washed ROS membranes and G $\beta 1\gamma 1$  were prepared from bovine retina as described previously (30,31).

*Construction, expression and purification of proteins*- Briefly, the pSV277 expression vector encoding Gai1 with N-terminal His-tag served as the template for introducing individual mutant substitutions using the QuickChange system (Stratagene). All mutations were confirmed by DNA sequencing (DNA Sequencing Facility, Vanderbilt University). The mutant constructs were then expressed and purified as previously described (32). The purified proteins were cleaved with thrombin (Sigma, 0.5 U/mg final concentration) for 16 hr at 4 °C in order to remove the N-terminal His-tag. The sample was then loaded onto a Ni-NTA column to separate the protein from the cleaved His-tag and any uncleaved fraction. For further purification, the protein solution was loaded onto size-exclusion column (TSKgel G2000SW) that was equilibrated in buffer A [50 mM Tris-HCl (pH 7.4), 150 mM NaCl, 2 mM MgCl<sub>2</sub>, 40  $\mu$ M GDP (or 1  $\mu$ M GTP $\gamma$ S), 2 mM DTT and 100  $\mu$ M PMSF]. SDS-

PAGE was used to test the purity of the proteins. Protein concentrations were determined by Bradford assay (33).

*Nucleotide-exchange assay*- The basal rate of GTP $\gamma$ S binding was determined by monitoring the relative increase in the intrinsic tryptophan (W211) fluorescence ( $\lambda_{ex}$  290 nm,  $\lambda_{em}$  340 nm) of Gai1 (200 nM) in buffer containing 50 mM Tris (pH 7.2), 100 mM NaCl and different amounts of MgCl<sub>2</sub> for 60 min at 25 °C after the addition of 10 mM GTP $\gamma$ S. Receptor mediated nucleotide exchange was determined with G $\beta 1\gamma 1$  (400 nM) in the presence of 50 nM rhodopsin at 21 °C for 60 min after the addition of GTP $\gamma$ S. The data were normalized to the baseline and maximum fluorescence and then fit to the exponential association equation ( $Y = Y_{max} * (1 - e^{-kt})$ ), to calculate the rate constant (k) as previously described (9).

*Intrinsic Trp fluorescence assay with AIF*- Intrinsic tryptophan (W211) fluorescence upon AIF<sub>4</sub><sup>-</sup> activation, relative to emission in the GDP bound state of G protein alpha subunit, was monitored as previously described (34). Data represent the averages from 6-8 experiments.

*Trypsin digestion and analysis*- 2  $\mu$ g Gai1 were incubated in buffer containing 50 mM Tris (pH 7.5), 100 mM NaCl, 20  $\mu$ M GDP and different amounts of MgCl<sub>2</sub> (0.5, 1, 2 mM). 10 mM NaF and 50  $\mu$ M AlCl<sub>3</sub> were added to samples, then incubated for 2 min at 25 °C. One microliter of a 1 mg/ml TPCK trypsin solution was added and incubated on ice for 25 min. The reaction was stopped by adding 2.5  $\mu$ l of termination solution (10 mg/ml aprotinin, 10 mM PMSF). Subsequently, samples were boiled with Laemmli sample buffer for 5 min, and run on a 12.5% SDS-polyacrylamide gel, stained with Coomassie Blue and quantified by densitometry (Multimager, Bio-Rad) (30,35,36).

*Cross-Linking*- An expression vector encoding Gai1 with six amino acid substitutions at solvent exposed cysteines (Gai1 HI) and an internal His6 tag between residues Met119 and Thr120 served as the template for introducing individual cysteine substitutions using the QuikChange system (Stratagene) as describe above. The bifunctional cross-linking reagent Bis-maleimidoethane (BMOE, Pierce Biotechnology) was incubated in a 2:1 molar ratio with Gai1 HI as previously

described (37). The concentrated, cross-linked monomeric protein was then purified by size exclusion chromatography on a calibrated G2000SW column. Calibration was performed under the same conditions as purification, using a broad range of molecular weight standards (Biorad) (37).

*Membrane binding assay-* The ability of mutant Ga subunits to bind rhodopsin in urea-washed ROS membranes was determined as previously described (9). Each sample was evaluated by comparison of the amount of G $\alpha 1$  subunit within the pellet (P) or supernatant (S) to the total amount of G $\alpha 1$  subunit (P+S) in both treatments expressed as a percentage of the total G $\alpha 1$  protein. Data represents the average of three experiments.

*Protein crystallization, data collection and structure determination-* Purified GDP bound Ga subunits were exchanged into crystallization buffer (50 mM EPPS (pH 8.0), 1 mM EDTA, 2 mM MgCl<sub>2</sub>, 5 mM DTT, 1 mM GDP) using a size exclusion chromatography column. Appropriate fractions were pooled as described above and SDS-PAGE was used to assess to test the purity of the proteins. Crystals were grown by the hanging drop vapor diffusion method at 18 °C by equilibration against a reservoir solution containing 2.0-2.3M (NH<sub>4</sub>)<sub>2</sub>SO<sub>3</sub> and 100mM sodium acetate (pH 5.9-6.4). Proteins (10 mg/ml) were mixed 1:2.5 ratio with reservoir solution and crystals appeared after 14-18 days with in the space group I4. A similar strategy was used to grow crystals G $\alpha 1$ -GTP $\gamma$ S proteins. Proteins were incubated with 10  $\mu$ M GTP $\gamma$ S for 30 min on ice and then storage buffer replaced the crystallization solution containing 50  $\mu$ M GTP $\gamma$ S instead of GDP. G $\alpha 1$ -GTP $\gamma$ S samples crystallized in the space group P3<sub>2</sub>21. Crystals were cryo-protected prior to data collection by briefly soaking in stabilization solution containing 18% Glycerol and 2.4 M (NH<sub>4</sub>)<sub>2</sub>SO<sub>3</sub> for ~30 s and cryo cooled by immersion in liquid nitrogen.

Data sets were collected at the LS-CAT (21-ID-G) of the Advanced Photon Source (APS) at Argonne National Laboratory at -180 °C using a wavelength of 0.98 Å on a MAR CCD detector. Data were processed and scaled using the HKL2000, CCP4 and Phenix suites (38-40). Crystallographic data processing and refinement

statistics are reported in **Table 1**. Criteria for data cutoff were a combination of R<sub>sym</sub> and I/ $\sigma$  which both rose to unacceptable levels if the resolution were extended by G $\alpha$ . The structures of G $\alpha 1$ -GDP and G $\alpha 1$ -GTP $\gamma$ S complexes were determined by molecular replacement using 1GDD (WT G $\alpha 1$ -GDP)(41) and 1GIA (G $\alpha 1$ -GTP $\gamma$ S·Mg<sup>2+</sup>)(42) as search models for Phaser-MR in the Phenix suite (40). Since 1GDD and 1GIA preceded the requirement for deposition of structural factors R-free reflections were randomly selected for F336C variant and was the same as F336Y. As a result, the free R is of limited utility. Model building was performed in Coot (43) using composite omit maps calculated in Phenix (40) to minimize model bias. Refinement conducted by both CNS (44) and Phenix, final refinements done by Phenix suite. In the final model, the regions corresponding to amino acids 1-8 and 203-211 in F336C-GDP, and 1-8, 202-217 and 233-240 in F336Y-GDP are not included. Similarly, in the GTP $\gamma$ S bound structures, amino acids 1-32 and 349-354 are not included due to lack of electron density. Structural superpositions were performed using Superpose for the C $\alpha$  carbon backbone in the CCP4 suite (45,46). All structural images were made with PyMOL (PyMOL Molecular Graphics System, Version 1.5.0.4 Schrödinger, LLC.) unless otherwise indicated.

## RESULTS

In this study, our strategy was to test residues around the  $\alpha 5$  helix that were previously identified as critical for the function of this helix during G protein activation. Residues were examined using biochemical, computational, and structural approaches in both basal and receptor bound state.

*The effects of  $\beta 5$ - $\beta 6$  strand mutants on G protein activation-* In our previous study, we proposed four residues that face the  $\alpha 5$  helix in  $\beta 5$  (I265, F267) and  $\beta 6$  (Y320, H322) (26). Any one of these might be critical for  $\alpha 5$  helix stability and therefore the G protein activation (**Fig. 2A**) (26). To test the effect of these residues on G protein function, we evaluated nucleotide exchange rates after introduction of site directed mutations. Basal and receptor mediated nucleotide exchange rates of mutants were determined by monitoring the relative increase in the intrinsic tryptophan (W211) fluorescence of G $\alpha 1$ . All of the mutants showed similar nucleotide exchange rates compare

to WT  $G\alpha 1$  in both receptor bound and unbound states (**Fig. 2B**). The simplest way to explain this data would be that those residues do not play a major role in G protein activation or that a single mutation is not enough to disturb the  $\alpha 5$  helix for GDP release. However, when we computed pairwise residue interactions, we identified interesting details for receptor mediated activation. In the basal state, I265, F267, Y320 and H322 were interacting hydrophobically with V339, V335, V342 and V335, respectively, within the  $\alpha 5$  helix. After receptor interaction and  $\alpha 5$  helix rotation, the same residues in  $\beta 5$  and  $\beta 6$  were predicted to hydrophobically interact with new sets of residues in the  $\alpha 5$  helix that were previously pointing toward solvent and not involved in binding in the basal state. Specifically I265, F267, Y320 and H322 started to interact with A338, N331, A338 and F334 respectively (**Fig. 2C&D, see Supplemental Table and Movie 1-3 for full data**). The  $\alpha 5$  helix can glide along this hydrophobic surface during its rotation. These calculations thus suggested how new interactions on the rotated the  $\alpha 5$  helix can possibly compensate for the effect of single mutations in  $\beta 5$  and  $\beta 6$  strands during receptor mediated G protein activation.

*The effects of F336 mutants on G protein activation-* To test the role of interactions with the opposite site of the  $\alpha 5$  helix post-rotation, we focused on one specific residue in the  $\alpha 5$  helix, phenylalanine 336 (F336). F336 is one of the highly conserved residues in the  $G\alpha$  protein family as well as the small GTPases. The side chain faces the  $\beta 1$ ,  $\beta 2$ , and  $\beta 3$  strands as well as the  $\alpha 1$  helix, which creates one of the conserved hydrophobic clusters in the  $G\alpha$  subunit. Our previous energetic study predicted that F336 is the most critical residue for both basal and receptor mediated G protein activation within the  $\alpha 5$  helix (**Fig. 3A & 3B**) (26). To test the effect of mutating this residue, we substituted F336 with residues with decreasing hydrophobicity. All of the F336 mutants displayed increased basal exchange rates compared to WT (**Fig. 3C**). Furthermore, a strong correlation was identified between the hydrophobicity of this residue and basal activity (**Fig. 3E**). The fastest nucleotide exchange rate was detected for F336Y. However, in receptor mediated activation, nucleotide exchange rates were decreased compared to WT without any

correlation with hydrophobicity (**Fig. 3D & 3F, Supplemental Movie 2&4**). This result is consistent with a rotation of  $\alpha 5$  leading to a new surface-exposed location of F336 during  $\alpha 5$  helix rotation and translation caused by interaction with the receptor (26). Overall these data suggest that F336 is one of the critical control points that regulate GDP release during G protein activation.

*The effects of F336 mutations on  $\beta 6$ - $\alpha 5$  loop; Cross-linking  $\alpha 1$  and  $\alpha 5$  helices-* The most obvious connection between the  $\alpha 5$  helix and the nucleotide binding pocket is the  $\beta 6$ - $\alpha 5$  loop. Perturbation of the  $\alpha 5$  helix during receptor-mediated activation would disturb the interaction between the  $\beta 6$ - $\alpha 5$  loop and the guanine ring of the nucleotide, leading to destabilization of the GDP in its binding pocket and domain opening of the  $\alpha$  subunit. To test the effect of F336 mutations on this loop, we cross-linked  $\alpha 1$  to  $\alpha 5$  to minimize the disruption of its interactions with the guanine ring by translocation toward the receptor. Cross-linking (XL) was performed between I56C-T329C residues on a cysteine depleted  $G\alpha 1$  ( $G\alpha 1$  HI) protein (**Fig. 4A**). Without cross-linking,  $G\alpha 1$  HI I56C-T329C showed higher basal nucleotide exchange rates compared with the  $G\alpha 1$  HI protein (**Fig. 4B**, black bars). Moreover, as expected, substitution of F336 for C on  $G\alpha 1$  HI I53C-T329C further increased the protein's activity. After cross-linking, the nucleotide exchange rate of cross-linked  $G\alpha 1$  XL HI I56C-T329C was decreased as compared to un-cross-linked proteins, demonstrating the stabilizing effect of the cross-linking. Substitution of F336C on cross-linked  $G\alpha 1$  HI I56C-T329C increased basal protein activation as compared to the uncross-linked  $G\alpha 1$  HI I56C-T329C-F336C mutant (**Fig. 4B**, black bars). This indicates that perturbation of F336 can trigger the activation mechanism without translocation of  $\alpha 5$  toward the receptor and disruption of  $\beta 6$ - $\alpha 5$  loop region.

Since receptor-mediated activation causes both a rotation of the  $\alpha 5$  helix as well as an uncoiling of one turn of helix, we expected the cross-linked  $G\alpha$  would be resistant to receptor-mediated activation. This is indeed what was found in both cross-linked proteins (**Fig. 4B**, grey bars). This result might be caused by the reduced capability of cross-linked  $G\alpha$  to interact with either  $G\beta\gamma$  subunits or the receptor. To test the first possibility, we measured the basal nucleotide

exchange rates of  $G\alpha$  mutants in the presence or absence of  $G\beta\gamma$  subunits (**Fig. 4C**). The results showed that basal nucleotide exchange rates decreased on both cross-linked and uncross-linked mutant  $G\alpha$  proteins in the presence of the  $G\beta\gamma$  subunit, like the WT protein. This suggested that cross-linked  $G\alpha$  subunits were still capable of interacting with  $G\beta\gamma$  subunits. To test the receptor binding capability of mutant  $G\alpha 1$  subunits, we determined the effect of cross-linking on the membrane association of the G protein with light-activated rhodopsin, a measure of the formation of the high-affinity R-G complex. As expected, cross-linking between  $\alpha 1$  and  $\alpha 5$  impaired this membrane binding (**Fig. 4D & E**), consistent with a lack of ability of the cross-linked  $\alpha 5$  helix to translocate towards the receptor and the decreased nucleotide exchange rates. Overall, the cross-linking data suggest that perturbation of F336 triggers GDP release through destabilization of SW I-II regions via perturbing the  $\alpha 5$  helix interactions along the  $\alpha 1$  helix and  $\beta 2$ - $\beta 3$  strands, rather than disrupting the  $\beta 6$ - $\alpha 5$  loop region.

*Hydrophobic interactions around F336:  $\alpha 1$  helix interface binding energy and G protein activation-* Previous data suggested that F336's interaction with the  $\alpha 1$  helix and  $\beta 2$ - $\beta 3$  strands might be crucial for domain opening as the  $\alpha 1$  helix is positioned at the interface of the  $G\alpha$ -GTPase domain and the helical domain (25). In addition, the  $\alpha 1$  helix and  $\beta 2$ - $\beta 3$  strands interact with the P-loop and SWI-II, respectively. To probe the effects of hydrophobic interactions around F336 with the  $\alpha 1$  helix, we computed interaction energies for all residues within the  $\alpha 1$  helix in both basal and receptor bound states of the heterotrimeric  $G\alpha\beta\gamma$  using our established protocol (26). These  $\Delta\Delta G$  values probed for a potential network of intramolecular interactions which could propagate the conformational changes necessary for G protein activation and nucleotide exchange.  $\Delta\Delta G$  calculations predicted the importance of  $\pi$ - $\pi$  interactions between the aromatic rings of F189 and H57 in the  $\beta 2$  strand and  $\alpha 1$  helix, respectively (**Fig. 5A, Table 2**). This pairwise interaction couples with F336 on the  $\alpha 5$  helix. Other predicted stabilizing interactions between  $\alpha 1$  (Q52 and I56) keep the  $\alpha 5$  helix (T329) fixed in the receptor unbound state; receptor interaction triggers unwinding of a turn of the  $\alpha 5$  helix, disturbing this interaction (**Fig. 5B,**

**Table 2**). On the face of  $\alpha 1$ , in contact with the helical domain, residues (K51, K54, I55, Y61, and L175) on both the  $\alpha 1$  and  $\alpha F$  helices assist to secure the helical domain in a "closed" GDP-bound conformation. The total interaction energy was approximately 25.4 Rosetta Energy Units (REUs). In the basal state, the  $\alpha 1$  helix was predicted to interact favorably with  $\beta 2$ - $\beta 3$  (F189, M198 and D200; 3.59 REU),  $\alpha 5$  (V332, F336; REU 2.44) and helical domain (E65, L175; 1.84 REU) (**Table 2**). In the receptor bound state, the  $\alpha 1$  helix was predicted to interact favorably with  $\alpha 5$  (N331, V332; 2.1 REU) and as expected, the overall interaction was calculated as lower than the unbound state (**Table 2**).

To test our computational results, we mutated two residues that are predicted to stabilize the  $\alpha 1$ - $\alpha 5$  interaction (F189 and F191). In the basal state, F189C increased nucleotide exchange 5-fold, while F191C showed no change relative to WT  $G\alpha 1$  (**Fig. 5C**). We prepared double and triple mutants with M53C and F196C mutants which we had previously tested (26). Double mutants (M53C-F189C and F189C-F196C) exhibited similar basal activation and a triple mutant (M53C-F189C-F196C) showed an even higher basal exchange rate compared to the F336C  $G\alpha 1$  mutant protein (**Fig. 5C**). In receptor mediated activation of exchange, there was again a pattern of only modest inhibition, with F191C showing the largest decrease (**Fig. 5D**) consistent with previously predicted  $\alpha 5$  (26) and  $\alpha 1$  interface binding energy calculations.

*Perturbation of phosphate site of nucleotide binding region with F336 mutants-* To determine if the hydrophobic pocket around F336 was necessary to control the local order of the phosphate binding region of GDP, we used the sensitive monitor of  $Mg^{2+}$  binding into this region. Three different strategies were used to investigate the influence of  $G\alpha 1$  mutants on  $Mg^{2+}$  binding to this region: a)  $[Mg^{2+}]$  effects on the kinetics of nucleotide exchange, b)  $AlF_4^-$  binding, and c) trypsin digestion of  $G\alpha 1$  in the presence of different concentrations of  $Mg^{2+}$ . The results showed that the high nucleotide exchange rates of the mutants could be decreased in elevated  $Mg^{2+}$  concentrations (**Fig. 6A & 6B**), suggesting that these mutations had allosteric effects on the phosphate binding region that could be overcome with higher  $Mg^{2+}$  concentration. The highest

decrease in the rate of exchange, as a function of increasing concentrations of  $Mg^{2+}$ , was observed for the F336Y mutant, which showed the fastest exchange rate in the presence of low  $Mg^{2+}$  concentrations (**Fig. 3C**).

To investigate the order of the  $Mg^{2+}$  binding region in the presence of GDP, the  $AIF_4^-$  binding assay was used. In this assay, changes in intrinsic tryptophan fluorescence rates of *Gai1* were measured upon  $AIF_4^-$  addition in the presence of different  $MgCl_2$  concentrations.  $Mg^{2+}$  is necessary for  $AIF_4^-$  binding and generation of the active or transition state. Thus, this assay reflects both  $AIF_4^-$  and  $Mg^{2+}$  coordination in that region without nucleotide exchange. All mutations showed destabilization effects that were overcome with increasing  $Mg^{2+}$  concentration. The  $EC_{50}$  for  $Mg^{2+}$  stabilization of  $AIF_4^-$  binding for F336M, F336C, F336A and F336Y was increased by 1.4, 2.1, 2.8 and 3.1 fold, respectively, over the WT *Gai1* under the same experimental conditions (**Fig. 6C**). In addition to the  $\alpha 5$  helix mutants, the M53C-F189C-F196C mutant also exhibited statistically significant increased  $EC_{50}$  (**Fig. 6C**).

The sensitivity of the *Gai1* mutants to the trypsin digestion assay is a complementary assay to show the subtle changes in local order at the trypsin digestion site at R208 in the presence of varying  $Mg^{2+}$  concentrations. After activation by either GDP- $AIF_4^-$  or GTP $\gamma$ S, *Gai1* yields a ~34 kDa fragment following trypsin digestion. All high nucleotide exchange mutants had reduced stability as assayed by decreased 34kDa fragment in the presence of low  $Mg^{2+}$  concentrations compared to the WT *Gai1* subunit (**Fig. 6D**).

*Structural features of the x-ray structures of the F336C and F336Y mutants-* To probe the structural basis for the increased rates of nucleotide exchange observed in the F336 mutants, the crystal structures of the F336C and F336Y variants of the *Gai1* subunit were determined in both the GDP and the GTP $\gamma$ S-bound states. The data collection and refinement statistics are summarized in **Table 1**. The mutations in the protein were confirmed by the crystal structure, where electron density at position 336 corresponded to either cysteine or tyrosine (**Fig. 7A & 7B**). The structures of the GDP-bound form of F336C and F336Y *Gai1* were refined to 2.0 and 2.4 Å resolution, respectively. Both GTP $\gamma$ S bound structures were refined to a resolution of 2.0 Å.

The GDP- and GTP $\gamma$ S-bound structures for F336C and F336Y were determined in space groups identical to those of the WT *Gai1* structures. Neither mutant showed significant structural differences compared to WT *Gai1*. Even with the F336 mutations in the  $\alpha 5$  helix, the crystal structures showed the same localization and similar average *B* (temperature) factors around F336 region relative to those of WT *Gai1* structures (**Fig. 7C**). The effects of F336 mutations on the  $\beta 2$ - $\beta 3$  strands and  $\beta 2$ - $\beta 3$  loop were minimal (**Fig. 7D & 7E**). Overall the root-mean square deviation (r.m.s.d) between WT *Gai1*-GDP with F336C and F336Y *Gai1*-GDP was 0.42 Å and 0.36 Å (310 C $\alpha$  atoms aligned out of 324 total), respectively, whereas it was 0.31 and 0.29 Å (304 C $\alpha$  atoms aligned out of 315) for their GTP $\gamma$ S-bound structures.

## DISCUSSION

The  $\alpha 5$  helix of the  $G\alpha$  subunit is a critical region for both the receptor-mediated and basal activity (1,9,14,15,18). It is encircled by hydrophobic interactions from six beta strands ( $\beta 1$ - $\beta 6$ ) and the  $\alpha 1$  helix ( $\alpha 1$ ). In the current study, we tested residues around the  $\alpha 5$  helix that we predicted as critical for the function of this helix during G protein activation in our previous studies. We highlight information flow within the G protein, starting from the  $\alpha 5$  helix to the GDP binding site of  $G\alpha$  using biochemical, structural and computational approaches.

Our previous study predicted that F336 within the  $\alpha 5$  helix is an important amino acid for both the active and inactive states (26); a finding consistent with other studies (14,28). Mutation of this residue resulted in constitutive activity in both monomeric and heterotrimeric G proteins (14,16,29,47). It is also known that in small GTPases, structural perturbation of that region through mutation causes increased guanine nucleotide turnover that can lead to several diseases; these include Noonan, Cardio-faciocutaneous and Costello syndromes (47-49).

In contrast to strong constitutive G protein activation, in this study, we did not observe drastic differences in the crystal structures of either GDP or GTP $\gamma$ S bound F336 mutants. Like another highly constitutively active G protein mutant, *Gai1* A326S (50), F336 mutants showed similar structural features compared to WT *Gai1*. The

guanine nucleotide provides a number of stabilizing interactions to the protein, perhaps inhibiting our ability to visualize subtle allosteric changes in the protein. In addition, other residues in the  $\alpha 5$  helix and  $\beta$ -strands may contribute in holding this region intact during the crystallization process.

How does the perturbation at F336 connect to the GDP binding region which is  $\sim 16$  Å removed? F336 is a part of a highly conserved hydrophobic core in the  $G\alpha$  subunit. The effect of F336 mutations on basal G protein activation is correlated with the hydrophobicity of this region (**Fig. 3C & 3E**). Once the receptor contacts the  $\alpha 5$  helix and causes its rotation and displacement into the receptor binding site, this F336 is now in a hydrophilic environment. We propose that breaking the hydrophobic core is a key event in perturbing GDP binding (26). Interestingly, we did not observe any effects of the hydrophilic mutants on receptor mediated activation; this is likely due to the new solvent exposed site which prevents these side chains from contacting anything other than solvent upon receptor binding (**Fig. 3D & 3F**).

To trace the hydrophobic interactions and to discern a possible interaction network from the F336 residue to the GDP binding site, we computed binding energies of different regions in the  $G\alpha$  subunit by using different Rosetta algorithms. Adding to our previous calculations ( $\alpha 5$  helix: $G\alpha$  interface binding energy, (26)), we predicted that the F336 side chain is mostly coupled with M53 ( $\alpha 1$ ), I56 ( $\alpha 1$ ), F189 ( $\beta 2$ ), F191 ( $\beta 2$ ), F196 ( $\beta 3$ ), V332 ( $\alpha 5$ ), Q333 ( $\alpha 5$ ), V339 ( $\alpha 5$ ) and T340 ( $\alpha 5$ ). Thus the effects of F336 are not solely local and not coupled to a single residue, but rather might be part of a distributed network of interactions in which the activation is coupled to changes in regions dispersed across both domains of the  $G\alpha$  subunit. F336 is likely making direct hydrophobic contacts with F191 and M53. It potentially communicates with F189 via two paths.

The first is through residues M53-H57-F191 which interact with F189 through a  $\pi$ - $\pi$  interaction between residues H57 and F189 (**Fig. 5A**). This is consistent with one of our previous studies (51) in which the constitutively active I56C( $\alpha 1$ )-Q333C( $\alpha 5$ ) double mutant of  $G\alpha 1$  made a spontaneous disulphide bond between the  $\alpha 1$  and

$\alpha 5$  helices. This structure showed significant rearrangement of side chain residues H57, F189, F191, and F332 and disturbed  $\pi$ - $\pi$  interaction between H57 and F189.

The second path begins from the direction of F196, which interacts with F336 via F191 and T340 residues. These observations indicate that the perturbation effects of F336 spread with complex interactions via the  $\alpha 1$  helix and  $\beta 2$ - $\beta 3$  strands. These interactions also spread to the  $Mg^{2+}$  ion and the nucleotide binding region (**Fig. 5 & 6**) as evidenced by our nucleotide exchange data combined with the perturbations seen in the  $Mg^{2+}$  and  $AlF_4^-$  assays which supports previous studies (8,16).

We also tested the effects of residues within the  $\beta 5$ - $\beta 6$  strands (I265 ( $\beta 5$ ), F267 ( $\beta 5$ ), Y320 ( $\beta 6$ ), H322 ( $\beta 6$ )) interacting with the other side of the  $\alpha 5$  helix on G protein activation. We observed no major effects from the mutations either in the basal or receptor mediated exchange assays. These data suggest how new interactions on the rotated  $\alpha 5$  helix can compensate for the effects of single mutations in the  $\beta 5$  and  $\beta 6$  strands during receptor mediated G protein activation. It also strongly suggests that the activation route goes through the other side of the protein (the  $\beta 1$ - $\beta 3$ / $\alpha 1$  to Switch I, P-loop,  $Mg^{2+}$  binding and GDP binding site), consistent with previously published findings (28). In addition, after restricting the C-terminal rotation and translocation by cross-linking the  $\alpha 1$  and  $\alpha 5$  helices, F336 mutants can still induce increased basal nucleotide exchange (**Fig. 4**). This observation indicates that G proteins do not need a large displacement of  $\alpha 5$  for basal state activation; rather, perturbing the  $\beta 2$ - $\beta 3$  and  $\alpha 1$  regions are sufficient.

In summary, our study used a predictive energetic analysis to pinpoint information flow through  $G\alpha$  from receptor interaction to triggering of GDP release. We highlighted the hydrophobic interactions around F336 as a key for stability of GDP binding, as well as removal of these hydrophobic interactions by receptor-mediated helical rotation to trigger GDP release. We suggested the route of information flow triggers through the  $\alpha 5$  helix,  $\beta 2$ - $\beta 3$  strands and the  $\alpha 1$  helix using energetic analysis and mutagenesis. We also showed that the dynamics of the  $Mg^{2+}$  and  $\beta$ -phosphate binding area of GDP are perturbed by mutagenesis of this conserved residue. The  $\beta 5$ - $\beta 6$

residues which face the  $\alpha 5$  helix are likely important structurally rather than functionally according to our analysis. Thus, our data suggest that after the initial interaction of the G protein with the receptor and CT rotation, disruption of a

conserved hydrophobic network around F336 engages both  $\beta 1$ - $\beta 3$  and  $\alpha 1$  to Switch I and the P-loop which decreases the stability of the GDP binding pocket and triggers nucleotide release.

## REFERENCES

1. Sprang, S. R. (1997) G Protein Mechanisms: Insights from Structural Analysis. *Annual Review of Biochemistry* **66**, 639-678
2. Higashijima, T., Ferguson, K. M., Smigel, M. D., and Gilman, A. G. (1987) The Effect of GTP and  $Mg^{2+}$  on the GTPase Activity and the Fluorescent Properties of  $G_o$ . *Journal of Biological Chemistry* **262**, 757-761
3. Oldham, W. M., and Hamm, H. E. (2007) How do receptors activate G proteins? *Adv Protein Chem* **74**, 67-93
4. Onrust, R., Herzmark, P., Chi, P., Garcia, P. D., Lichtarge, O., Kingsley, C., and Bourne, H. R. (1997) Receptor and  $\beta\gamma$  Binding Sites in the  $\alpha$  Subunit of the Retinal G Protein Transducin. *Science* **275**, 381-384
5. Hamm, H. E. (1998) The Many Faces of G protein Signaling. *Journal of Biological Chemistry* **273**, 669-672
6. Rasmussen, S. G., Choi, H. J., Rosenbaum, D. M., Kobilka, T. S., Thian, F. S., Edwards, P. C., Burghammer, M., Ratnala, V. R., Sanishvili, R., Fischetti, R. F., Schertler, G. F., Weis, W. I., and Kobilka, B. K. (2007) Crystal structure of the human beta2 adrenergic G-protein-coupled receptor. *Nature* **450**, 383-387
7. Rosenbaum, D. M., Rasmussen, S. G., and Kobilka, B. K. (2009) The structure and function of G-protein-coupled receptors. *Nature* **459**, 356-363
8. Scheerer, P., Park, J. H., Hildebrand, P. W., Kim, Y. J., Krauss, N., Choe, H. W., Hofmann, K. P., and Ernst, O. P. (2008) Crystal structure of opsin in its G-protein-interacting conformation. *Nature* **455**, 497-502
9. Oldham, W. M., Van Eps, N., Preininger, A. M., Hubbell, W. L., and Hamm, H. E. (2006) Mechanism of the receptor-catalyzed activation of heterotrimeric G proteins. *Nat Struct Mol Biol* **13**, 772-777
10. Okada, T., Fujiyoshi, Y., Silow, M., Navarro, J., Landau, E. M., and Shichida, Y. (2002) Functional role of internal water molecules in rhodopsin revealed by X-ray crystallography. *Proceedings of the National Academy of Sciences of the United States of America* **99**, 5982-5987
11. Ernst, O. P., Bieri, C., Vogel, H., and Hofmann, K. P. (2000) Intrinsic biophysical monitors of transducin activation: fluorescence, UV-visible spectroscopy, light scattering, and evanescent field techniques. *Methods Enzymol* **315**, 471-489
12. Hamm, H. E., Deretic, D., Arendt, A., Hargrave, P. A., Koenig, B., and Hofmann, K. P. (1988) Site of G Protein Binding to Rhodopsin Mapped with Synthetic Peptides from the  $\alpha$  Subunit. *Science* **241**, 832-835
13. Palczewski, K., Kumasaka, T., Hori, T., Behnke, C. A., Motoshima, H., Fox, B. A., Le Trong, I., Teller, D. C., Okada, T., Stenkamp, R. E., Yamamoto, M., and Miyano, M. (2000) Crystal structure of rhodopsin: A G protein-coupled receptor. *Science* **289**, 739-745
14. Marin, E. P., Krishna, A. G., and Sakmar, T. P. (2001) Rapid Activation of Transducin by Mutations Distant from the Nucleotide-Binding Site. Evidence for a Mechanistic Model of Receptor-Catalyzed Nucleotide Exchange by G Proteins. *Journal of Biological Chemistry* **276**, 27400-27405
15. Marin, E. P., Krishna, A. G., and Sakmar, T. P. (2002) Disruption of the  $\alpha 5$  Helix of Transducin Impairs Rhodopsin-Catalyzed Nucleotide Exchange. *Biochemistry* **41**, 6988-6994
16. Kapoor, N., Menon, S. T., Chauhan, R., Sachdev, P., and Sakmar, T. P. (2009) Structural evidence for a sequential release mechanism for activation of heterotrimeric G proteins. *J Mol Biol* **393**, 882-897
17. Bourne, H. R. (1997) How receptors talk to trimeric G proteins. *Current Opinion in Cell Biology* **9**, 134-142

18. Rasmussen, S. G., Devree, B. T., Zou, Y., Kruse, A. C., Chung, K. Y., Kobilka, T. S., Thian, F. S., Chae, P. S., Pardon, E., Calinski, D., Mathiesen, J. M., Shah, S. T., Lyons, J. A., Caffrey, M., Gellman, S. H., Steyaert, J., Skiniotis, G., Weis, W. I., Sunahara, R. K., and Kobilka, B. K. (2011) Crystal structure of the beta(2) adrenergic receptor-Gs protein complex. *Nature* **477**, 549-555
19. Westfield, G. H., Rasmussen, S. G., Su, M., Dutta, S., DeVree, B. T., Chung, K. Y., Calinski, D., Velez-Ruiz, G., Oleskie, A. N., Pardon, E., Chae, P. S., Liu, T., Li, S., Woods, V. L., Jr., Steyaert, J., Kobilka, B. K., Sunahara, R. K., and Skiniotis, G. (2011) Structural flexibility of the G alpha s alpha-helical domain in the beta2-adrenoceptor Gs complex. *Proc Natl Acad Sci U S A* **108**, 16086-16091
20. Abdulaev, N. G., Ngo, T., Zhang, C., Dinh, A., Brabazon, D. M., Ridge, K. D., and Marino, J. P. (2005) Heterotrimeric G-protein alpha-subunit adopts a "preactivated" conformation when associated with betagamma-subunits. *J Biol Chem* **280**, 38071-38080
21. Oldham, W. M., Van Eps, N., Preininger, A. M., Hubbell, W. L., and Hamm, H. E. (2007) Mapping allosteric connections from the receptor to the nucleotide-binding pocket of heterotrimeric G proteins. *Proc Natl Acad Sci U S A* **104**, 7927-7932
22. Iiri, T., Farfel, Z., and Bourne, H. R. (1998) G-protein diseases furnish a model for the turn-on switch. *Nature* **394**, 35-38
23. Cherfils, J., and Chabre, M. (2003) Activation of G-protein  $G\alpha$  subunits by receptors through  $G\alpha$ - $G\beta$  and  $G\alpha$ - $G\gamma$  interactions. *Trends in Biochemical Sciences* **28**, 13-17
24. Rondard, P., Iiri, T., Srinivasan, S., Meng, E., Fujita, T., and Bourne, H. R. (2001) Mutant G protein  $\alpha$  subunit activated by  $G\beta\gamma$ : A model for receptor activation? *Proceedings of the National Academy of Sciences of the United States of America* **98**, 6150-6155
25. Louet, M., Martinez, J., and Floquet, N. (2012) GDP release preferentially occurs on the phosphate side in heterotrimeric G-proteins. *PLoS Comput Biol* **8**, e1002595
26. Alexander, N. S., Preininger, A. M., Kaya, A. I., Stein, R. A., Hamm, H. E., and Meiler, J. (2014) Energetic analysis of the rhodopsin-G-protein complex links the alpha5 helix to GDP release. *Nat Struct Mol Biol* **21**, 56-63
27. Marin, E. P., Krishna, A. G., Archambault, V., Simuni, E., Fu, W. Y., and Sakmar, T. P. (2001) The Function of Interdomain Interactions in Controlling Nucleotide Exchange Rates in Transducin. *Journal of Biological Chemistry* **276**, 23873-23880
28. Ceruso, M. A., Periole, X., and Weinstein, H. (2004) Molecular Dynamics Simulations of Transducin: Interdomain and Front to Back Communication in Activation and Nucleotide Exchange. *Journal of Molecular Biology* **338**, 469-481
29. Johnston, C. A., Willard, M. D., Kimple, A. J., Siderovski, D. P., and Willard, F. S. (2008) A sweet cycle for Arabidopsis G-proteins: Recent discoveries and controversies in plant G-protein signal transduction. *Plant signaling & behavior* **3**, 1067-1076
30. Mazzoni, M. R., Malinski, J. A., and Hamm, H. E. (1991) Structural Analysis of Rod GTP-binding Protein,  $G_t$ . Limited Proteolytic Digestion Pattern of  $G_t$  with Four Proteases Defines Monoclonal Antibody Epitope. *Journal of Biological Chemistry* **266**, 14072-14081
31. Thaker, T. M., Kaya, A. I., Preininger, A. M., Hamm, H. E., and Iverson, T. M. (2012) Allosteric mechanisms of G protein-Coupled Receptor signaling: a structural perspective. *Methods Mol Biol* **796**, 133-174
32. Medkova, M., Preininger, A. M., Yu, N. J., Hubbell, W. L., and Hamm, H. E. (2002) Conformational Changes in the Amino-Terminal Helix of the G Protein  $\alpha_{i1}$  Following Dissociation from  $G\beta\gamma$  Subunit and Activation. *Biochemistry* **41**, 9962-9972
33. Bradford, M. M. (1976) A rapid and sensitive method for the quantitation of microgram quantities of protein utilizing the principle of protein-dye binding. *Anal Biochem* **72**, 248-254

34. Coleman, D. E., and Sprang, S. R. (1998) Crystal Structures of the G Protein  $G_{i\alpha 1}$  Complexed with GDP and  $Mg^{2+}$ : A Crystallographic Titration Experiment. *Biochemistry* **37**, 14376-14385
35. Schmidt, C. J., Thomas, T. C., Levine, M. A., and Neer, E. J. (1992) Specificity of G Protein  $\beta$  and  $\gamma$  Subunit Interactions. *Journal of Biological Chemistry* **267**, 13807-13810
36. Linder, M. E., Middleton, P., Hepler, J. R., Taussig, R., Gilman, A. G., and Mumby, S. M. (1993) Lipid modifications of G proteins: alpha subunits are palmitoylated. *Proc Natl Acad Sci U S A* **90**, 3675-3679
37. Van Eps, N., Preininger, A. M., Alexander, N., Kaya, A. I., Meier, S., Meiler, J., Hamm, H. E., and Hubbell, W. L. (2011) Interaction of a G protein with an activated receptor opens the interdomain interface in the alpha subunit. *Proc Natl Acad Sci U S A* **108**, 9420-9424
38. Otwinowski, Z., and Minor, W. (1997) Processing of X-ray Diffraction Data Collected in Oscillation Mode. in *Macromolecular Crystallography Part A* (Carter, C. W., Jr., and Sweet, R. M. eds.), Academic Press, New York. pp 307-326
39. Potterton, E., Briggs, P., Turkenburg, M., and Dodson, E. (2003) A graphical user interface to the CCP4 program suite. *Acta Crystallographica Section D* **59**, 1131-1137
40. Adams, P. D., Afonine, P. V., Bunkoczi, G., Chen, V. B., Davis, I. W., Echols, N., Headd, J. J., Hung, L.-W., Kapral, G. J., Grosse-Kunstleve, R. W., McCoy, A. J., Moriarty, N. W., Oeffner, R., Read, R. J., Richardson, D. C., Richardson, J. S., Terwilliger, T. C., and Zwart, P. H. (2010) PHENIX: a comprehensive Python-based system for macromolecular structure solution. *Acta Crystallographica Section D* **66**, 213-221
41. Mixon, M. B., Lee, E., Coleman, D. E., Berghuis, A. M., Gilman, A. G., and Sprang, S. R. (1995) Tertiary and Quaternary Structural Changes in  $G_{i\alpha 1}$  Induced by GTP Hydrolysis. *Science* **270**, 954-960
42. Coleman, D. E., Berghuis, A. M., Lee, E., Linder, M. E., Gilman, A. G., and Sprang, S. R. (1994) Structures of Active Conformations of  $G_{i\alpha 1}$  and the Mechanism of GTP Hydrolysis. *Science* **265**, 1405-1412
43. Emsley, P., and Cowtan, K. (2004) Coot: model-building tools for molecular graphics. *Acta Crystallographica Section D* **60**, 2126-2132
44. Brunger, A. T., Adams, P. D., Clore, G. M., DeLano, W. L., Gros, P., Grosse-Kunstleve, R. W., Jiang, J. S., Kuszewski, J., Nilges, M., Pannu, N. S., Read, R. J., Rice, L. M., Simonson, T., and Warren, G. L. (1998) Crystallography & NMR system: A new software suite for macromolecular structure determination. *Acta Crystallogr D Biol Crystallogr* **54**, 905-921
45. Winn, M. D., Ballard, C. C., Cowtan, K. D., Dodson, E. J., Emsley, P., Evans, P. R., Keegan, R. M., Krissinel, E. B., Leslie, A. G., McCoy, A., McNicholas, S. J., Murshudov, G. N., Pannu, N. S., Potterton, E. A., Powell, H. R., Read, R. J., Vagin, A., and Wilson, K. S. (2011) Overview of the CCP4 suite and current developments. *Acta Crystallogr D Biol Crystallogr* **67**, 235-242
46. Krissinel, E., and Henrick, K. (2004) Secondary-structure matching (SSM), a new tool for fast protein structure alignment in three dimensions. *Acta Crystallogr D Biol Crystallogr* **60**, 2256-2268
47. Quilliam, L. A., Zhong, S., Rabun, K. M., Carpenter, J. W., South, T. L., Der, C. J., and Campbell-Burk, S. (1995) Biological and structural characterization of a Ras transforming mutation at the phenylalanine-156 residue, which is conserved in all members of the Ras superfamily. *Proc Natl Acad Sci U S A* **92**, 1272-1276
48. Sovik, O., Schubert, S., Houge, G., Steine, S. J., Norgard, G., Engelsen, B., Njolstad, P. R., Shannon, K., and Molven, A. (2007) De novo HRAS and KRAS mutations in two siblings with short stature and neuro-cardio-facio-cutaneous features. *Journal of medical genetics* **44**, e84

49. Schubbert, S., Bollag, G., Lyubynska, N., Nguyen, H., Kratz, C. P., Zenker, M., Niemeyer, C. M., Molven, A., and Shannon, K. (2007) Biochemical and functional characterization of germ line KRAS mutations. *Mol Cell Biol* **27**, 7765-7770
50. Posner, B. A., Mixon, M. B., Wall, M. A., Sprang, S. R., and Gilman, A. G. (1998) The A326S mutant of G $\alpha$ 1 as an approximation of the receptor-bound state. *J Biol Chem* **273**, 21752-21758
51. Preininger, A., Funk, M., Meier, S., Oldham, W., Johnston, C., Adhikary, S., Kimple, A., Siderovski, D., Hamm, H., and Iverson, T. (2009) Helix dipole movement and conformational variability contribute to allosteric GDP release in G $\alpha$ i subunits. *Biochemistry* **48**, 2630-2642
52. Oldham, W. M., and Hamm, H. E. (2006) Structural basis of function in heterotrimeric G proteins. *Q Rev Biophys* **39**, 117-166
53. Chen, V. B., Arendall, W. B., 3rd, Headd, J. J., Keedy, D. A., Immormino, R. M., Kapral, G. J., Murray, L. W., Richardson, J. S., and Richardson, D. C. (2010) MolProbity: all-atom structure validation for macromolecular crystallography. *Acta Crystallogr D Biol Crystallogr* **66**, 12-21

*Acknowledgments*-We thank Jin Liao for her excellent technical assistance.

## FOOTNOTES

The work in the author's laboratories was supported in whole or in part by the National Institutes of Health grants EY006062 (to H.E.H.), GM095633 (to T.M.I.), GM080403, MH090192, GM099842, DK097376 (to J.M.), S10 RR026915 (to Vanderbilt Robotic Crystallization facility) and National Institutes of Science grants BIO Career 0742762 and CHE 1305874 (to J.M.). Use of the Advanced Photon Source, an Office of Science User Facility operated for the U.S. Department of Energy (DOE) Office of Science by Argonne National Laboratory, was supported by the U.S. DOE under Contract No. DE-AC02-06CH11357. Use of the LS-CAT Sector 21 was supported by the Michigan Economic Development Corporation and the Michigan Technology Tri-Corridor (Grant 085P1000817).

Atomic coordinates and structure factors have been deposited into the RCSB Protein Data Bank with accession codes 4PAN, 4PAM, 4PAO and 4PAQ.

The abbreviations used are:

APS	Advanced Photon Source
BMOE	Bis-maleimidoethane
GDP	Guanosine diphosphate
GPCR	G Protein Coupled Receptor
GTP $\gamma$ S	Guanosine 5'-[ $\gamma$ -thio]triphosphate
LS-CAT	Life Sciences Collaborative Access Team
P-loop	phosphate binding loop
REU	Rosetta Energy Units
r.m.s.d	root mean square deviation
ROS	rod outer segment

## FIGURE LEGENDS

**FIGURE 1. Heterotrimeric G protein; localization and function  $\alpha 5$  helix in G proteins.** (A) Ribbon model of heterotrimeric G protein ( $G_{i\alpha\beta\gamma}$ , PDB entry, 1GP2). The  $G_{\alpha}$  subunit is composed of nucleotide binding (GTPase domain, light blue) and helical domains (green). The  $\alpha 5$  helix and switch regions are colored yellow and purple, respectively. GDP is shown as sticks. (B) Receptor (orange) mediated G protein activation routes. The binding of the GPCR to the C-terminus (CT) of  $G_{\alpha}$  is thought to trigger conformational changes that can be transmitted via rotation of the  $\alpha 5$  helix (black, arrow 1) of  $G_{\alpha}$  to the  $\beta 6$ - $\alpha 5$  loop (purple, arrow 2) that binds the purine ring of the GDP. In the second route, disruption of the phosphate interactions with the nucleotide binding pocket via destabilization of SW I-II regions through perturbing  $\alpha 5$  interaction with the  $\beta 2$ - $\beta 3$  strands (arrow 3). Rhodopsin –  $G_i$  complex model adapted from Alexander et.al. (26). (C and D) The  $\alpha 5$  helix is one of the most critical regions for G protein stability and activation. (A and B) The  $\alpha 5$  helix (yellow) is protected by six beta strands ( $\beta 1$ - $\beta 6$ ) and one  $\alpha$  helix ( $\alpha 1$ ) (green). The structure is adapted from the crystal structure of the  $G_i$  heterotrimer (PDB entry, 1GP2).

**FIGURE 2. The effects of  $\beta 5$ - $\beta 6$  strands mutations on G protein activation.** (A) Rosetta energy analysis of the interface between the  $\alpha 5$  helix (black) and the GTPase domain in the receptor bound state. Residues are colored by the interaction energy as reported in REU, or Rosetta Energy Units (dark blue, the most attractive). Calculations adapted from (26). (B) Basal (black bars) and receptor (grey bars) mediated nucleotide exchange rates for the  $\beta 5$  strand (I265A and F267A) and  $\beta 6$  strand (Y320C and H322A) mutations in *Gai1* proteins. Nucleotide exchange was monitored by measuring the enhancement in intrinsic tryptophan (W211) fluorescence (ex 290 nm, em 340 nm) as a function of time after addition of  $\text{GTP}\gamma\text{S}$  (52). (C) Most favorable interactions between the  $\alpha 5$  helix (V335, V339 and V342),  $\beta 5$  strand (I265 and F267), and  $\beta 6$  strand (T320 and H322) interface in the basal state. (D) After receptor interaction and  $\alpha 5$  helix rotation (arrow), the same residues in  $\beta 5$  and  $\beta 6$  were hydrophobically interacting with new residues in the  $\alpha 5$  helix (red labeled). Please see Supplemental Table and Supplemental Movie 1-3 for full interactions in both receptor bound and unbound states.

**FIGURE 3. The effect of F336 residue on G protein activation.** Rosetta energy analysis of the interface between the  $\alpha 5$  helix and GTPase domain in the basal state (A) and receptor bound state (B). Residues are colored by the interaction energy REU (dark blue, the most attractive). Calculations adapted from (26). Basal (C) and Receptor mediated (D) nucleotide exchange rates of *Gai1* F336 mutants. The data were normalized to the baseline and maximum fluorescence and then fit to the exponential association equation ( $Y = Y_{\text{max}} * (1 - e^{-kt})$ ), to calculate rate constant (k). Data were collected at 21 °C for 60 min. Results represent the mean  $\pm$  SEM values of at least three independent experiments. Correlation between nucleotide exchange rates and hydrophobicity identity of the amino acids in basal (E) and receptor bound (F) state. Engelman Scale was used during comparison and correlation coefficients were calculated with or without F336Y mutant data. The Pearson correlation in the basal state with F336Y is 0.9358; without F336Y, it is 0.9945. In receptor mediated state Pearson correlation with F336Y is 0.6992, without F336Y is 0.4861.

**FIGURE 4. Cross-linking of  $\alpha 1$  and  $\alpha 5$  helices of *Gai1* HI.** (A) Cartoon representation of cross-linking (XL) region. Cross-linking was performed between I56C ( $\alpha 1$ ) and T329C ( $\alpha 5$ ) (purple) residues on a cysteine depleted *Gai1* (*Gai1* HI) protein. F336 ( $\alpha 5$ ) residue is colored red, F189 ( $\beta 2$ ), F191 ( $\beta 2$ ), F196 ( $\beta 3$ ) and M53 ( $\alpha 1$ ) residues are colored green. The  $\alpha 5$  helix is colored yellow, the  $\beta 1$ - $\beta 6$  strands and  $\alpha 1$  helix are colored green. (B) Basal (black bars) and receptor (grey bars) mediated nucleotide exchange rates for cross-linked *Gai1* HI proteins. (C) Basal nucleotide exchange rates in the presence of  $\text{G}\beta\gamma$  subunit.  $\text{G}\alpha$  (black bars),  $\text{G}\alpha\beta\gamma$  (shaded black bars). (D) Membrane binding of wild type and mutant *Gai1* HI proteins. Assay was performed as described in method section. DS, supernatant from dark sample; DP, pellet fraction from dark sample; LS, supernatant from light sample; LP, pellet from light sample; GS, supernatant from light- and  $\text{GTP}\gamma\text{S}$ -activated sample; GP, pellet from light- and  $\text{GTP}\gamma\text{S}$ -activated sample; XL, cross-linked sample. (E) Densitometric quantification of supernatant from light samples. Each sample from SDS-PAGE (section d) was evaluated by comparison of the amount of *Gai1* subunits in pellet (P) or supernatant (S) to the total amount of *Gai1* subunits (P+S) in both treatments and expressed as a percentage of the total *Gai1* protein. Data represents the average of three independent experiments.

**FIGURE 5. The effects of hydrophobic residues around F336 on nucleotide exchange rates.** Rosetta energetic analysis of the interface between  $\alpha 1$  helix and GTPase domain in the basal state (A) and receptor bound state (B). Residues are colored by the interaction energy in REU (dark blue, the most attractive). Basal (C) and receptor mediated (D) nucleotide exchange rates of single, double and triple mutants within the  $\beta 2$ - $\beta 3$  strands and  $\alpha 1$  helix as determined by monitoring intrinsic tryptophan (W211) fluorescence changes upon addition of  $\text{GTP}\gamma\text{S}$ . Data were collected at 21 °C for 45 min. Results represent the mean  $\pm$  SEM values of at least three independent experiments.

**FIGURE 6. The effect of  $MgCl_2$  on *Gai1* basal activity.** (A) Basal nucleotide exchange in the presence 2 mM and 10 mM  $MgCl_2$  concentrations. (B) Changes in the nucleotide exchange rate in the presence of different  $MgCl_2$  concentrations. Fold change calculated from (A) and normalized with *Gai1* (WT) data. (C) Rates of intrinsic tryptophan fluorescence changes in *Gai1* upon aluminum fluoride ( $AlF_4^-$ ) addition in the presence of different  $MgCl_2$  concentrations (0.1-2 mM). Intensity of tryptophan signal were monitored (ex: 290 nm, em: 340 nm) at 21 °C for 10 min before and after the addition of  $AlF_4^-$  (10 mM NaF and 50  $\mu$ M  $AlCl_3$ ). The data were calculated as described above and rate constants plotted against  $MgCl_2$  concentrations. (D) Trypsin digestion and analysis of *Gai1* protein subunit. The densitometric measurement of proteolytic fragments in the presence of GDP -  $AlF_4^-$  + 0.5 mM  $MgCl_2$ . Results normalized with WT *Gai1* data and fragments quantified by densitometry (Multimager, Bio-Rad). Results represent the mean  $\pm$  SEM values of at least 6-8 independent experiments.

**FIGURE 7. Structural features of GDP bound F336 mutant structures.** Electron density for the F336C (A) and F336Y (B) side chains in the GDP bound state of  $G\alpha 1$ . Corresponding regions in GDP-bound WT *Gai1* (PDB entry, 1GDD (41); teal) are superposed. Difference electron density is from a |Fo|-|Fc| omit map calculated after the removal of residue 330 to 340 and contoured to  $3\sigma$  around the omitted side chain. (C) Comparison of the  $\alpha 5$  helix between F336C-GDP (white), F336Y-GDP (yellow) and WT *Gai1*-GDP (PDB entry, 1GDD, teal). (D) Overview of the  $\beta 2$ - $\beta 3$  strands and  $\beta 2$ - $\beta 3$  loop. (E) Comparison of relative localization of F189 ( $\beta 2$ ), F191 ( $\beta 2$ ), F196 ( $\beta 3$ ) and F336 ( $\alpha 5$ ) residues between F336C-GDP (white), F336Y-GDP (yellow) and WT- $G\alpha 1$  (PDB entry, 1GDD, teal) structures.

**Table 1. Crystallographic data collection and refinement statistics.**

	<b>F336C-GDP</b>	<b>F336C-GTP<math>\gamma</math>S</b>	<b>F336Y-GDP</b>	<b>F336Y-GTP<math>\gamma</math>S</b>
<b>Data Collection and Processing<sup>a</sup></b>				
Beamline	21-ID-G	21-ID-G	21-ID-G	21-ID-G
Space groups	I4	P3 <sub>2</sub> 21	I4	P3 <sub>2</sub> 21
Cell Dimensions: a, b, c (Å)	121.1, 121.1, 68.18	79.2, 79.2, 107.9	121.5, 121.5, 68.2	79.3, 79.3, 105.1
$\alpha, \beta, \gamma$ (degrees)	90, 90, 90	90, 90, 120	90, 90, 90	90, 90, 120
Resolution (Å)	34-2.1 (2.18-2.1)	31-2.0 (2.07-2.0)	20-2.4 (2.5-2.4)	42-2.0 (2.07-2.0)
Total Reflections	255,402	307,412	177,466	437,402
Unique Reflections	28,903	26,186	19,617	26,483
R <sub>sym</sub> <sup>b</sup> (%)	5.3 (37.9)	10.1 (44.7)	6.2 (32)	10.2 (44.6)
R <sub>pim</sub> <sup>c</sup> (%)	2.9 (23.2)	5.2 (23.5)	3.3 (18.4)	4.7 (20.7)
<I>/< $\sigma$ >	19.9 (2.6)	13.5 (3.1)	19.3 (3.46)	17.5 (3.9)
Completeness (%)	99.6 (99.5)	100 (100)	99.3 (99)	100 (100)
<b>Refinement Statistics</b>				
R <sub>work</sub> <sup>d</sup> (%)	18.8	16.4	18.2	16.9
R <sub>free</sub> (%)	21.8	20.8	23.2	20.6
RMS deviations				
Bond (Å)	0.008	0.007	0.008	0.007
Angle (°)	1.029	0.981	1.011	1.009
Ramachandran statistics <sup>e</sup>				
Favored (%)	98.5	99.06	98.11	98.42
Allowed (%)	1.5	0.94	1.89	1.58
Outliers (%)	0.0	0.0	0.0	0.0

<sup>a</sup>Numbers in parentheses indicate statistics for the highest shell.

<sup>b</sup> $R_{sym} = \sum |I_i - (I)| / \sum |I_i|$  where  $I$  is intensity,  $I_i$  is the  $i$ th measurement, and  $(I)$  is the weighted mean of  $I$ .

<sup>c</sup> $R_{pim} = \sum_{hkl} \sqrt{[1/(N-1)] \sum_i |I_i(hkl) - \overline{I(hkl)}|} / \sum_{hkl} \sum_i I_i(hkl)$  where  $I$  is running over the number of independent observations of reflection  $hkl$  and  $N$  is representing the number of replicate observations.

<sup>d</sup> $R_{work} = \sum ||Fo| - |Fc|| / \sum |Fo|$  where  $Fo$  and  $Fc$  are the observed and calculated structure factor amplitudes.  $R_{free}$  is the same as  $R_{work}$  for a set of data omitted from the refinement.

<sup>e</sup>Ramachandran analysis from MOLPROBITY (53).

Table 2. G protein alpha subunit  $\alpha 1$  helix interface energetic prediction

Free $G\alpha$					Receptor – $G\alpha$ complex				
Entity	Amino acid	Energy in REU	Std. dev	Z-score	Entity	Amino acid	Energy in REU	Std. dev	Z-score
$\beta 1$	L038	0.87	$\pm 0.04$	22.75	$\beta 1$	L038	0.78	$\pm 0.16$	4.85
$\alpha 1$	K046	1.14	$\pm 0.28$	4.01	$\beta 1$	G040	0.72	$\pm 0.34$	2.12
$\alpha 1$	S047	0.95	$\pm 0.04$	21.55	$\alpha 1$	K046	1.58	$\pm 0.41$	3.88
$\alpha 1$	T048	1.82	$\pm 0.05$	38.27	$\alpha 1$	S047	0.71	$\pm 0.14$	5.01
$\alpha 1$	I049	0.99	$\pm 0.09$	11.42	$\alpha 1$	I049	1.11	$\pm 0.1$	10.77
$\alpha 1$	K051	0.82	$\pm 0.1$	8.10	$\alpha 1$	V050	0.75	$\pm 0.16$	4.61
$\alpha 1$	Q052	1.65	$\pm 0.05$	34.32	$\alpha 1$	K051	0.52	$\pm 0.34$	1.55
$\alpha 1$	M053	1.33	$\pm 0.11$	12.04	$\alpha 1$	Q052	1.08	$\pm 0.13$	8.03
$\alpha 1$	K054	2.49	$\pm 0.07$	38.00	$\alpha 1$	M053	1.62	$\pm 0.15$	10.72
$\alpha 1$	I055	1.03	$\pm 0.16$	6.53	$\alpha 1$	K054	0.94	$\pm 0.45$	2.11
$\alpha 1$	I056	1.07	$\pm 0.03$	32.77	$\alpha 1$	I056	1.18	$\pm 0.2$	5.85
$\alpha 1$	H057	1.73	$\pm 0.08$	22.03	$\alpha 1$	H057	1.20	$\pm 0.57$	2.12
Helical	E065	0.78	$\pm 0.11$	6.96	$\beta 2$	F189	1.43	$\pm 0.17$	8.56
Helical	L175	1.06	$\pm 0.08$	13.10	$\beta 2$	F191	0.55	$\pm 0.08$	6.60
$\beta 2$	F189	1.41	$\pm 0.09$	15.72	$\alpha 5$	N331	1.02	$\pm 0.04$	23.43
$\beta 3$	M198	0.50	$\pm 0.12$	4.28	$\alpha 5$	V332	0.68	$\pm 0.08$	8.11
$\beta 3$	D200	0.81	$\pm 0.33$	2.45	GDP		0.70	$\pm 0.19$	3.79
$\beta 6$ - $\alpha 5$	A326	1.62	$\pm 0.04$	41.26	GDP	cumulative	0.70		
$\beta 6$ - $\alpha 5$	T329	0.82	$\pm 0.02$	41.22	$\alpha 1$	cumulative	10.69		
$\alpha 5$	V332	0.85	$\pm 0.03$	31.85	$\alpha 5$	cumulative	1.70		
$\alpha 5$	F336	0.72	$\pm 0.05$	15.83	$\beta$ -strands	cumulative	3.48		
GDP		0.95	$\pm 0.13$	7.32	overall	cumulative	16.57		
GDP	cumulative	0.95							
$\alpha 1$	cumulative	15.02							
Helical	cumulative	1.84							
$\beta 6$ - $\alpha 5$	cumulative	2.44							
$\alpha 5$	cumulative	1.57							
$\beta$ -strands	cumulative	3.59							
overall	cumulative	25.43							

Figure 1

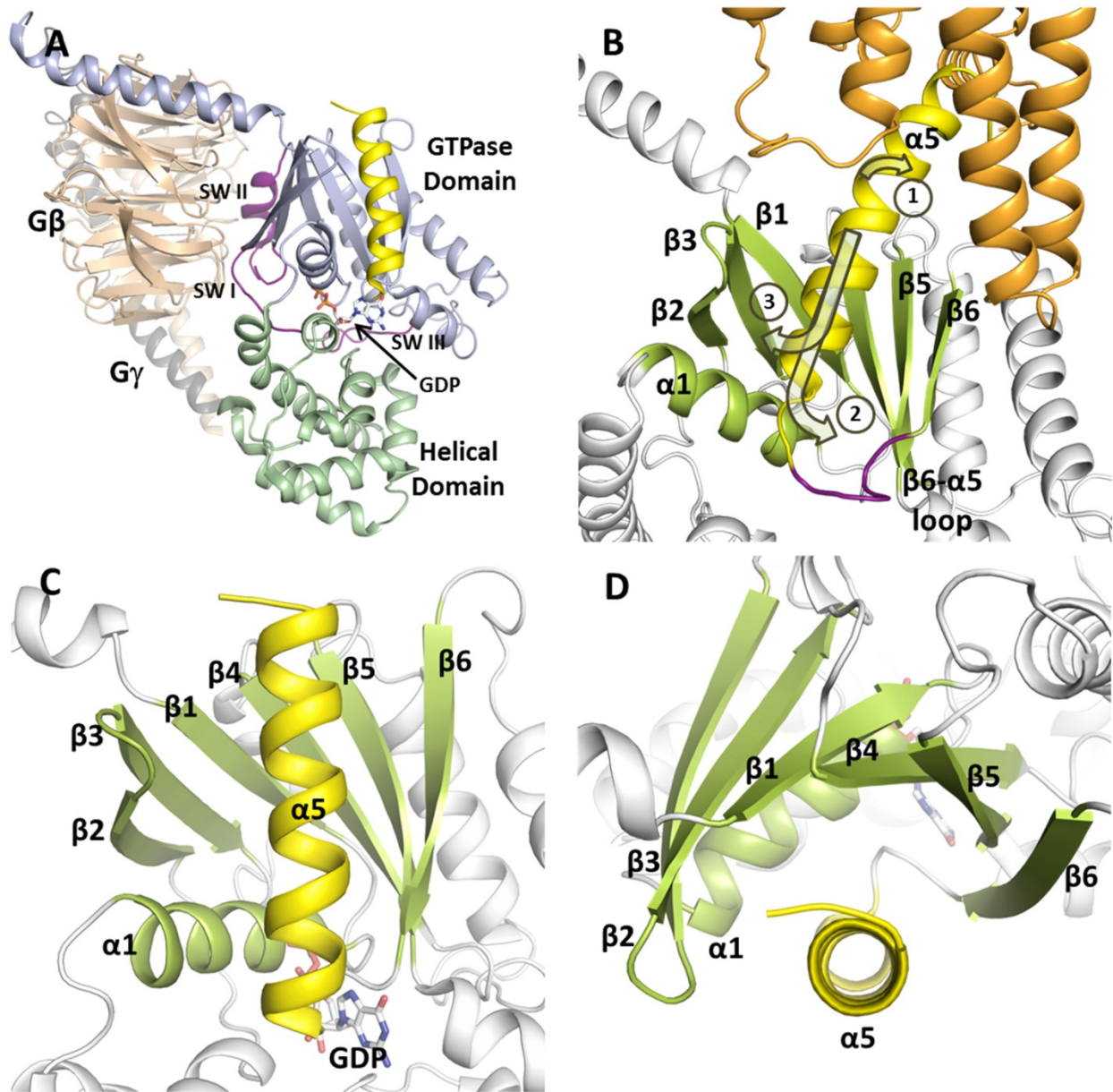


Figure 2

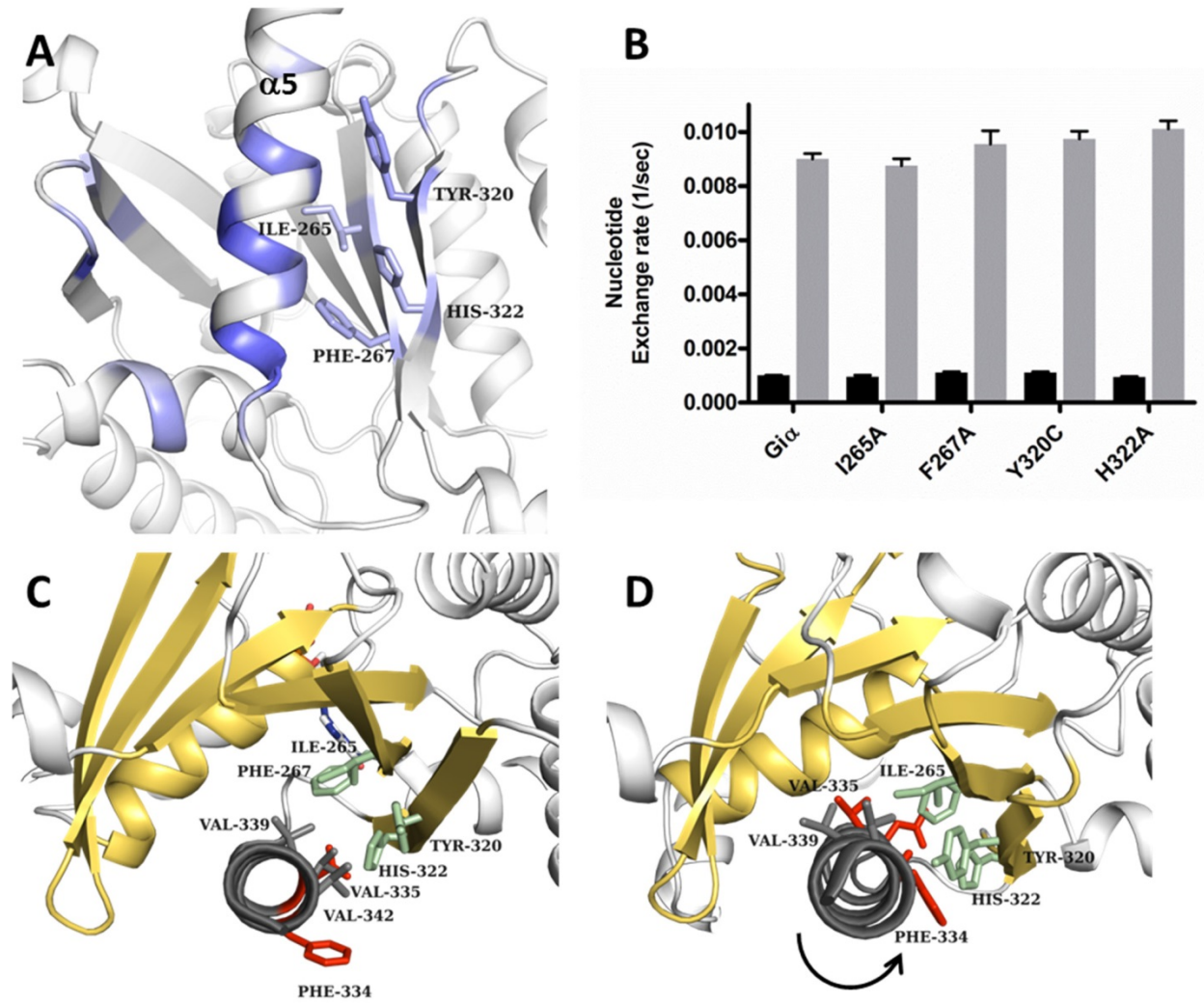


Figure 3

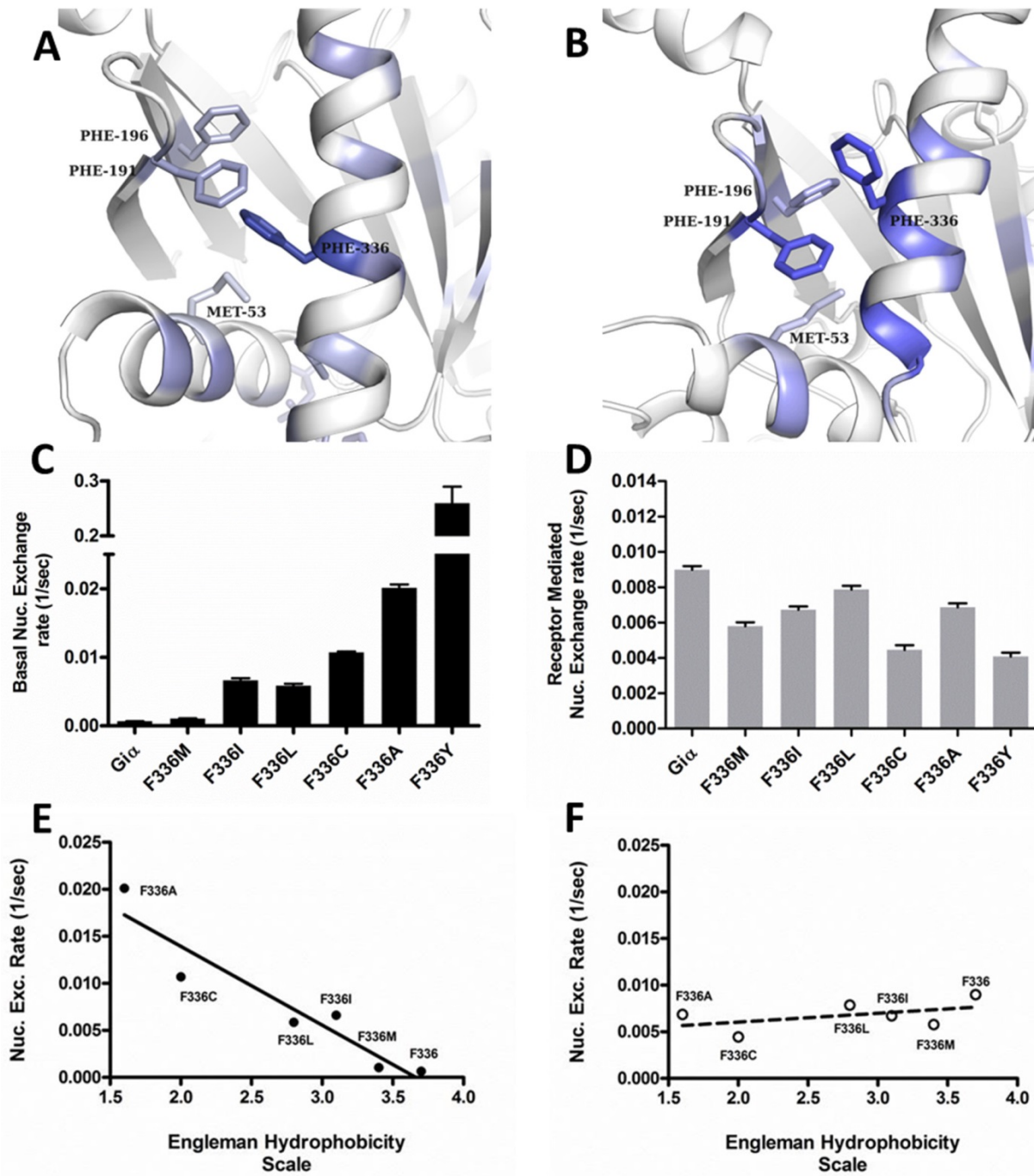


Figure 4

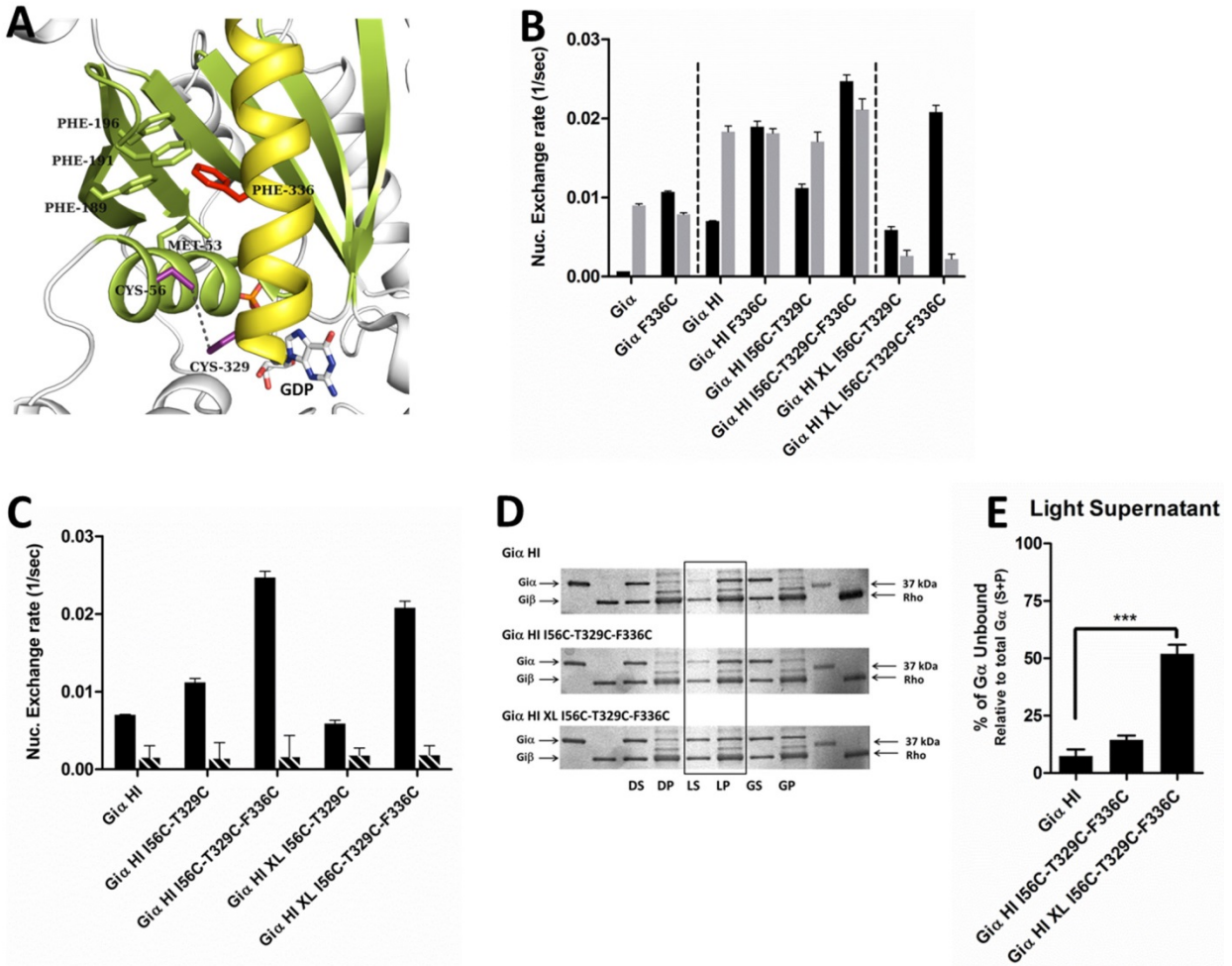


Figure 5

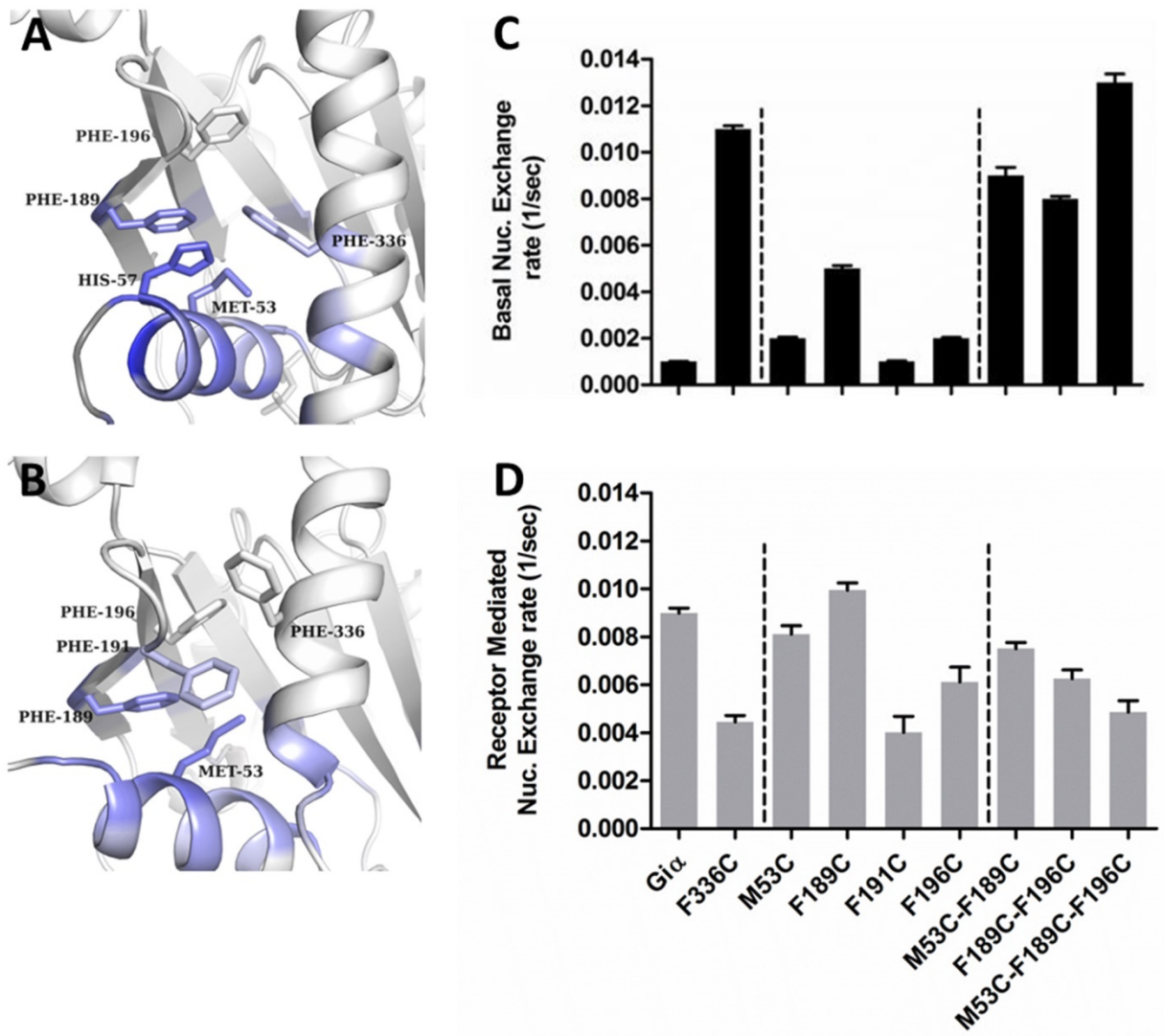


Figure 6

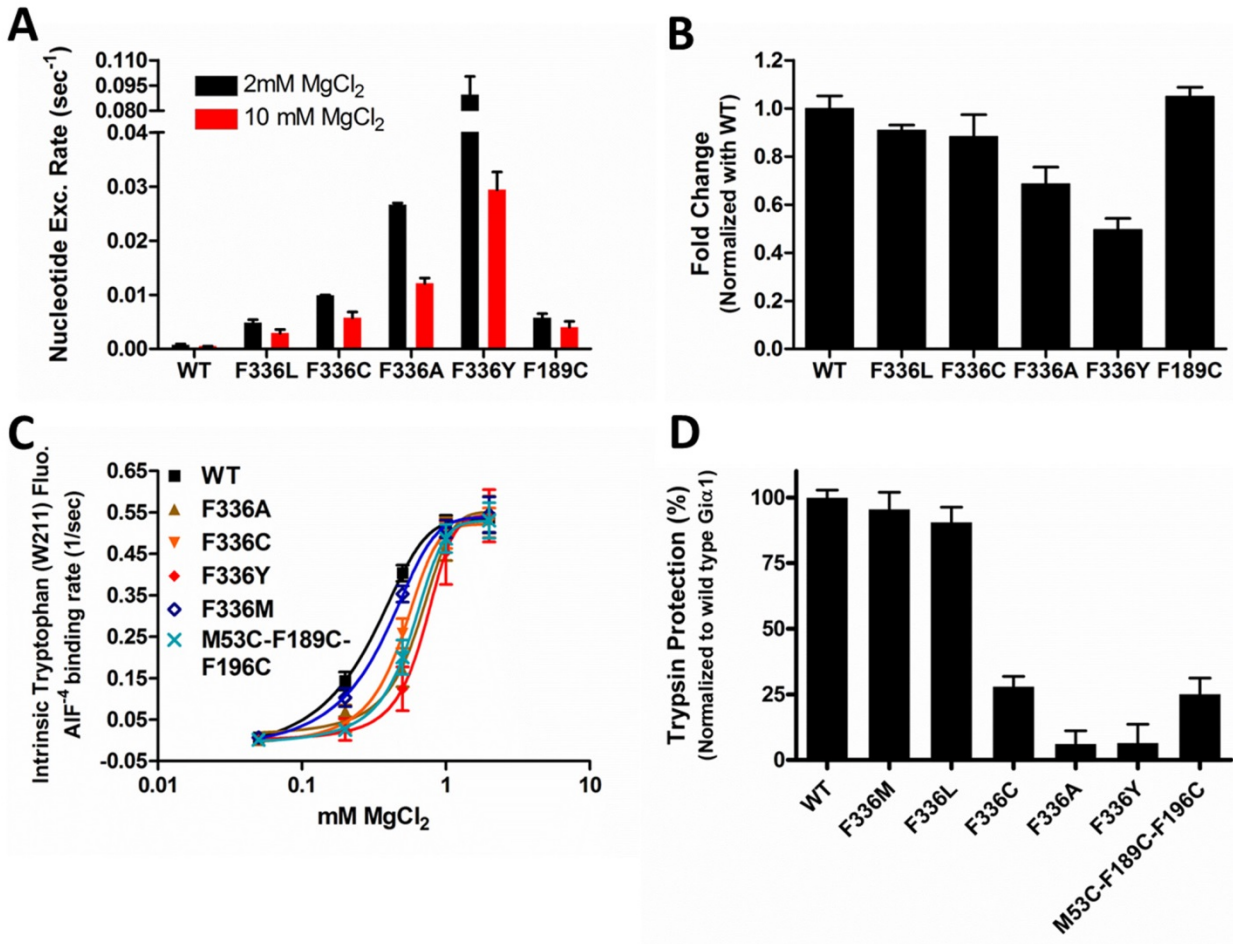


Figure 7

